Centerline computation and geometric analysis of branching tubular surfaces with application to blood vessel modeling

Luca Antiga
antiga@marionegri.it

Bogdan Ene-Iordache
bogdan@marionegri.it

Andrea Remuzzi
aremuzzi@marionegri.it

Bioengineering Department
Mario Negri Institute for Pharmacological Research
24020 Ranica (BG), Italy

Abstract

In this work we present a robust and accurate method for the computation of centerlines inside branching tubular objects starting from a piecewise linear representation of their boundary. The algorithm is based on solving the Eikonal equation on the Voronoi diagram embedded into the object, with wavefront speed inversely proportional to Voronoi ball radius values. As a result, provably accurate centerlines and maximal inscribed ball radius values along them are provided. In the same framework, a method for local surface characterization is also developed, allowing robust computation of the distance of surface points to centerlines and disclosing the relationship of surface points with centerlines. A new surface-based quantity is finally proposed, the *normalized tangency deviation*, which provides a scale-invariant criterion for surface characterization. The developed methods are applied to 3D models of vascular segments in the context of patient-specific anatomical characterization.

Keywords

Centerline, shape analysis, Voronoi diagram, Eikonal equation, Fast Marching Method, blood vessel modeling.

1 Introduction

Given the influence of geometry on fluid dynamics and the great inter-individual anatomic variability of blood vessels, characterization of blood vessel geometry is an important step towards a better understanding of the factors involved in vascular pathology. This kind of analysis must be performed at different levels of detail – synthetic parameters quantifying geometric features, such as stenosis grade, are required in diagnostic imaging; vessel axis definition and local radius measurement are important to synthesize the geometry of the vascu-

lar surface, in order study how different vessel global configurations undergo different pathological histories on populations of subjects; local geometric characterization of vessel surface is necessary to document the progression of vascular disease and to look for typical local geometric features associated with disease initiation.

In this work we present a method to perform centerline computation, local radius measurement and local surface characterization in a single framework, and in a robust and accurate way. Our starting point is a polygonal surface representing the vascular wall. Our technique is based on solving weighted geodesic problems on an approximation of the medial axis of tubular objects.

2 Methods

2.1 Centerline computation

Centerline can be defined as the line drawn between two sections of a tubular structure which maximize the distance from the boundary. The problem of centerline computation inside an object $\Omega \subset \Re^3$ can therefore be

formulated as looking for a path $\mathbf{C} = \mathbf{C}(s)$ traced between two points $\mathbf{p}_1$ and $\mathbf{p}_2$ for which the following functional

$$\mathcal{E}_{centerline}(\mathbf{C}) = \int_{0=\mathbf{C}^{-1}(\mathbf{p}_0)}^{L=\mathbf{C}^{-1}(\mathbf{p}_1)} F(\mathbf{C}(s))ds \qquad (1)$$

is minimal, where $F(\mathbf{x})$ is a scalar field which is lower for more internal points, for example a decreasing function of the distance transform associated with Ω, defined as

$$\mathrm{DT}(\mathbf{x}) = \min_{\mathbf{y} \in \partial\Omega} \{|\mathbf{x}, \mathbf{y}|\} \qquad (2)$$

where $|,|$ denotes the Euclidean distance, and $\partial\Omega$ the boundary of Ω. It is possible to demonstrate [Ant03] that by choosing $F(\mathbf{x}) = \mathrm{DT}^{-1}(\mathbf{x})$, centerlines defined as in Equation 1 lie on the medial axis of Ω, $\mathrm{MA}(\Omega)$, defined as the locus of centers of the maximal inscribed balls in Ω, where an inscribed ball is maximal if it is not strictly contained in any other inscribed ball. Dealing with piecewise linear approximations of $\partial\Omega$, a method to obtain an approximation of the medial axis of Ω is to compute the embedded Voronoi diagram of a point set P densely sampling $\partial\Omega$ ([AM97]). The Voronoi diagram of P is defined as

$$\mathrm{Vor}(P) = \bigcup_{\mathbf{p} \in P} \partial V(\mathbf{p}) \qquad (3)$$

where $V(\mathbf{p})$ is the Voronoi region associated with point $\mathbf{p}$, defined as

$$V(\mathbf{p}) = \left\{ \mathbf{x} \in \Re^3 : |\mathbf{p}, \mathbf{x}| \leq |\mathbf{q}, \mathbf{x}| \; \forall \mathbf{q} \in P \right\} \qquad (4)$$

In 3D, the Voronoi diagram is a non-manifold surface made up of convex polygons, whose vertices are the centers of the maximal emtpy balls with respect to point set P, whose radius is indicated by $R(\mathbf{x})$. Computation of the embedded Voronoi diagram was performed by first computing the Delaunay tessellation of P, $\mathrm{Del}(P)$, removing the tetrahedra whose circumcenter falls outside the object (using outward surface normals) and then constructing only those Voronoi polygons whose vertex loops are complete.

We then solved the problem in Equation 1 on the embedded Voronoi diagram, taking $F(\mathbf{x}) = R^{-1}(\mathbf{x})$, with an approach similar to that presented in [DC01] for the computation of centerlines in 3D images. As shown in [CK97], the strong formulation of Equation 1 is the Eikonal equation

$$|\nabla T(\mathbf{x})| = F(\mathbf{x}) \qquad (5)$$

with boundary condition $T(\mathbf{p}_0) = 0$. Equation 5 is a nonlinear partial hyperbolic equation that models first arrival times of a wavefront propagating over the domain with speed $F^{-1}(\mathbf{x})$. A very effecient method for the solution of the Eikonal equation is the Fast Marching Method ([Set99]), based on upwind finite-difference approximation, originally developed for orthogonal grids and successively extended to triangulated manifolds ([KS98]). In order to solve the problem on the Voronoi diagram, we extended the Fast Marching Method to polygonal non-manifolds [Ant03], in which more than two polygons can share a point or an edge. Once the Eikonal equation is solved over the whole Voronoi diagram with boundary condition $T(\mathbf{p}_0) = 0$, centerlines are obtained by backtracing a path from $\mathbf{p}_1$ along the direction of maximum descent of $T(\mathbf{x})$. The resulting centerline is a piecewise linear line defined on $\mathrm{Vor}_E(P)$, whose vertices lie on Voronoi polygon boundaries. Moreover, values of Voronoi sphere radius $R(\mathbf{x})$ are defined on centerlines, so that centerline points are associated with maximal inscribed spheres.

2.2 Geometric analysis

In this section we show how the techniques introduced so far can be further developed to geometrically characterize the surface of interconnected tubular objects. We do that by relating centerlines to surface points (and vice-versa) on the embedded Voronoi diagram domain. The idea is to take advantage of Voronoi diagram topology in evaluating the distance from surface points to centerlines, therefore overcoming the problems arising when simply calculating minimum Euclidean distance in complex geometries. The method is subdivided into two steps, the first of which is computing the distance from embedded Voronoi diagram points to centerlines, and the second finding a correspondence between surface points and embedded Voronoi diagram points.

Computation of the distance, measured on the embedded Voronoi diagram, from embedded Voronoi diagram points to centerlines is performed by solving the Eikonal equation

$$|\nabla \tilde{T}(\mathbf{x})| = 1 \qquad \forall \mathbf{x} \in \mathrm{Vor}_E(P) \qquad (6)$$

with boundary condition $\tilde{T}(\mathbf{C}) = 0$, where $\mathbf{C}$ stands for centerlines. Equation 6 returns the geodesic distance field $\tilde{T}(\mathbf{x})$ on each point of $\mathrm{Vor}_E(P)$.

The correspondence between surface points and embedded Voronoi diagram points is then given in terms of *poles*. The poles of a surface point are defined as its farthest inner and outer Voronoi vertices ([ACK01]). Since we are working with the embedded Voronoi diagram, only the inner fathest Voronoi vertex is considered, here denoted as $\mathbf{pole}(\mathbf{p})$. In 3D the set of poles of P converges to the medial axis of Ω when sampling density tends to infinity ([ACK01]). Moreover, the direction $(\mathbf{pole}(\mathbf{p}) - \mathbf{p})$ approximates the inward surface normal in $\mathbf{p}$, and leads from $\mathbf{p}$ to to the *deepest* Voronoi vertex around $\mathbf{p}$. As a result, we define the geodesic

distance from surface points to centerlines as

$$D_g(\mathbf{p}) = |\mathbf{pole}(\mathbf{p}) - \mathbf{p}| + \tilde{T}(\mathbf{pole}(\mathbf{p})) \qquad (7)$$

Correspondence between surface points and centerlines is then performed by tracing a path from each surface point $\mathbf{p}$ to $\mathbf{pole}(\mathbf{p})$, and from that to centerlines following the steepest descent of $\tilde{T}(\mathbf{x})$. The endpoint $\mathbf{c}(\mathbf{p})$ of the path starting in $\mathbf{p}$ is therefore the centerline point geodesically nearest to $\mathbf{p}$. Once $\mathbf{c}(\mathbf{p})$ is identified, the Euclidean distance of surface points to centerlines can be computed as $D_e(\mathbf{p}) = |\mathbf{c}(\mathbf{p}) - \mathbf{p}|$. From such correspondence, surface points can be characterized according to their belonging to different centerline branches or to the position along centerlines.

Last, we define a new surface-based quantity, named *normalized tangency deviation*, as

$$\mathrm{NTD}(\mathbf{p}) = \frac{\tilde{T}(\mathbf{pole}(\mathbf{p}))}{D_g(\mathbf{p})} \qquad (8)$$

which is a normalized measure of how far a surface is from being tangent to a maximal inscribed ball at a given point $\mathbf{p}$, independently from object scale. It is possible to demonstrate that for a cylinder with elliptical base NTD only depends on ellipse eccentricity [Ant03]. NTD is therefore a scale-independent parameter for the characterization of surface features.

3   Results

We first validated the techniques presented above applying them to circular and elliptical base cylinders for different aspect ratios of the base ellipses (see Table 1), and for different sampling point densities (see Table 2). The results show that the algorithm performance decreases when the section has a low aspect ratio. This is due to the fact that in these cases $F(\mathbf{x})$ is near to be constant over the medial axis around the centerline, so that line position is more sensitive to numerical artifacts. The correctedness of the interpretation is confirmed by the fact that maximal inscribed ball radius is accurately computed even in low aspect ratio models. As to dependence from point sampling density, the results show how the algorithm is very roust when the section is circular, while for lower aspect ratio elliptical sections a good performance relies on an adequate surface sampling density. It must be noted, however, how the density required for accurate results is not high (30 points on section edge, which roughly means one point every 12 degrees along the section edge). High maximal inscribed ball radius measurement error for elliptical base cylinders of low mesh density is caused by the fact that in this case Voronoi balls are not tangent to the surface, but rather intersect it between sampling points, thus overestimating real inscribed ball radius.

Aspect ratio	Error % $[\mu(\sigma)]$	
	Centerline	Radius
5/5	0.01(0.02)	0.03(0.06)
4/5	0.24(0.19)	0.33(0.04)
3/5	0.84(0.78)	0.57(0.04)
2/5	2.17(1.34)	0.96(0.17)

Table 1: Validation results for elliptical base cylinders of different aspect ratio (semiminor to semimajor ratio). Percent errors of centerline position and maximal inscribed ball radius along centerline are normalized against cylinder maximum and minimum radius respectively.

	Vertex no edge(tot)	Error % $[\mu(\sigma)]$		Time (s)
		Centerline	Radius	
A	40(2975)	0.01(0.02)	0.03(0.06)	12.34
	30(1693)	0.02(0.03)	0.10(0.15)	5.86
	20(757)	0.02(0.04)	0.25(0.35)	1.97
	10(198)	0.44(0.33)	1.38(1.20)	0.31
B	40(3628)	0.84(0.78)	0.57(0.04)	6.20
	30(2073)	0.74(0.72)	1.01(0.08)	3.18
	20(934)	2.88(1.95)	2.08(0.19)	1.21
	10(239)	4.42(4.68)*	7.48(0.79)	0.26

Table 2: Validation results for circular (A) and elliptical (aspect ratio 3/5) (B) base cylinders of different surface mesh density. Percent errors of centerline position and maximal inscribed ball radius along centerline are normalized against cylinder maximum and minimum radius respectively.
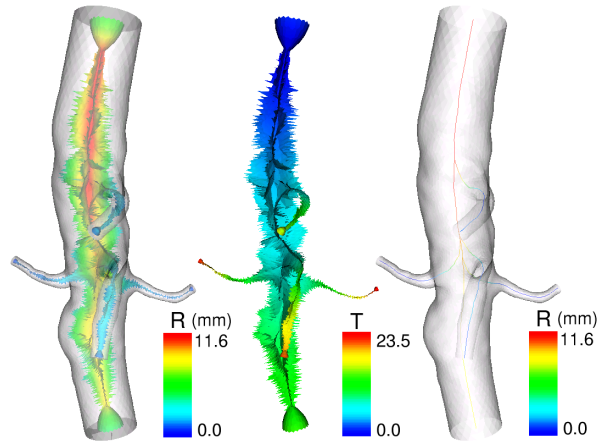
Figure 1: Left: abdominal aorta model and its embedded Voronoi diagram; colors represent Voronoi ball radius values. Middle: solution of the Eikonal equation from aorta inlet (upper outermost section) on the Voronoi diagram. Right: centerlines backtraced from the outlets to the inlet.
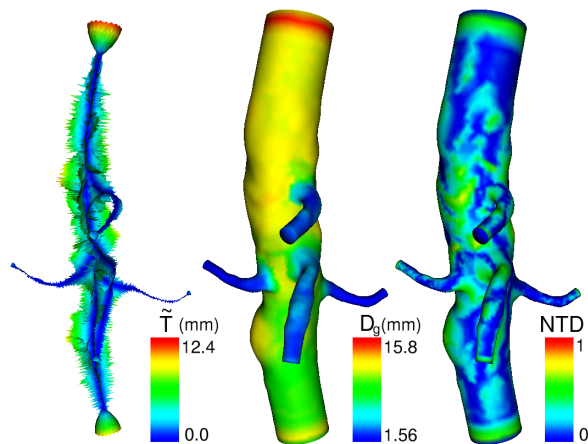
Figure 2: Left: solution of the Eikonal equation with unit speed from the centerlines on the Voronoi diagram. Middle: geodesic distance of surface points to centerlines D_g. Right: NTD distribution.

Figure 3: Maximal inscribed balls along a centerline for the abdominal aorta model. Left and middle: the same sphere is depicted from two different orientations.

We then applied the presented techniques to a model of abdominal aorta reconstructed from contrast-enhanced 3D MR angiography using a level set approach. The steps leading to the computation of centerlines are shown in Fig. 1, while geometric characterization phase is depicted in Fig. 2. It is worth to note how normalized tangency deviation distribution is effective in evidencing surface irregularities in a scale-indepentent way.

Maximal inscribed balls are depicted in Fig. 3 in two positions along the centerline traced from aorta inlet to celiac outlet. In particular, Fig. 3 left and middle depict the same sphere viewed in two different projections, evidencing the relationship from maximal inscribed ball radius measurement and minium projection diameter measurement, which is employed in the clinical practice on classic angiographic images. Minimum projection diameter measurement in fact consists in finding the minimum diameter of a vessel in a given position among angiographic images taken from different orientations.

4 Discussion

In this work we presented a general approach to characterize the geometry of objects composed of interconnecting tubular structures given their boundary surface. The method relies on solving weighted geodesics computation problems over the approximation of the object medial axis. Centerlines are computed accurately and in a robust way and local surface characterization with respect to the computed centerlines is provided in the same framework.

The methods are currently employed in the field of geometric analysis of vascular structures, in order to characterize patient-specific vascular anatomy and document the alterations due to pathological conditions, such as atherosclerotic plaque or aneurysm evolution.

References

[ACK01] N. Amenta, S. Choi, and R. K. Kolluri. The power crust. In *Proceedings of Solid Modeling '01*, pages 249–260, 2001.

[AM97] D. Attali and A. Montanvert. Computing and simplifying 2D and 3D continuous skeletons. *Computer vision and image understanding*, 67(261-273), 1997.

[Ant03] L. Antiga. *Patient-specific modeling of geometry and blood flow in large arteries*. PhD thesis, Politecnico di Milano, 2003.

[CK97] L. D. Cohen and R. Kimmel. Global minimum of active contour models: a minimal path approach. *International Journal of Computer Vision*, 24(1):57–78, Aug 1997.

[DC01] T. Deschamps and L. D. Cohen. Fast extraction of minimal paths in 3D images and application to virtual endoscopy. *Medical Image Analysis*, 5(4):281–299, Dec 2001.

[KS98] R. Kimmel and J. A. Sethian. Computing geodesic paths on manifolds. *Proceedings of National Academy of Sciences*, 95(15):8431–8435, Jul 1998.

[Set99] J. A. Sethian. *Level Set Methods and Fast Marching Methods*. Cambridge University Press, 2nd edition, 1999.